Journal of Building Engineering 39 (2021) 102309

Contents lists available at ScienceDirect

Journal of Building Engineering

journal homepage: http://www.elsevier.com/locate/jobe

Seismic performance factors of a dual system with IMRF and cable-cylinder bracing

Marzyeh Ghasemi [a], Nader Fanaie [b,*], Hossein Khorshidi [b]

[a] Department of Civil Engineering, Babol Noushirvani University of Technology, Mazandaran, Iran
[b] Department of Civil Engineering, K. N. Toosi University of Technology, Tehran, Iran

ARTICLE INFO

Keywords:
Cable-cylinder bracing
FEMA P695 methodology
Seismic performance factors (SPFs)
Incremental dynamic analysis (IDA)
Nonlinear static analyses (pushover)

ABSTRACT

In recent years, numerous approaches have been adopted to improve the performance of structural systems during earthquakes. Cable-cylinder bracing is an innovative displacement-restraint bracing method using wire ropes or cables that are bundled together with a cylinder at their junction. As designing structures with cable-cylinder braces based on the current design guidelines requires design parameters for the system, in this study, Seismic Performance Factors (SPFs) consists of the response modification factor (R), the over-strength factor (Ω_0), and the deflection amplification factor (C_d) are quantified according to the methodology proposed by FEMA P695. Following this procedure, a set of 2-, 4-, 6-, and 8-story archetypes were designed based upon presumed SPFs. The performance of each archetype was then examined through conducting nonlinear static analysis (pushover) and Incremental Dynamic Analysis (IDA). Collapse probability of archetypes by utilizing fragility curves and considering uncertainty sources have been assessed. Required parameters were evaluated for the designed archetypes and the values were compared with the accepted criteria to confirm the initial assumed SPFs for the cable-cylinder bracing system.

1. Introduction

Generally, steel Moment Resisting Frames (MRFs) exhibit ductile behavior, and unexpected events such as earthquakes might cause considerable story displacements in these structural systems. This issue has highlighted the significance of increasing story stiffness and strength. Over the past years, a multitude of approaches have been adopted to improve the performance of MRFs during earthquakes. Due to the monetary and constructional advantages, Concentrically Braced Frames (CBFs) are widely employed to increase the lateral stiffness and strength of the frames [1], and several studies investigated the seismic behavior and the design rules of such systems [2,3].

Cables are unique structural components to be used in the construction industry. Despite the high tensional strength and stiffness of steel cables, they are not proper alternatives in cross-bracing frames as a result of low ductility.

To tackle this problem, Hou and Tagawa [4] introduced a cable-cylinder bracing system. As shown in Fig. 1, two diagonal cables are bundled with a cylinder at their junction. Despite the classical MRF-CBF dual systems, in this innovative system, both cables tolerate only tension force. So, the loosening and the impulses of cables will be prevented. Moreover, in usual MRF-CBF, braces participate in energy dissipation (through the formation of the plastic hinge in the bracing), but in this system, cables and steel cylinder remain elastic and do not play any role in energy dissipation. Furthermore, in classical MRF-CBF, collapse occurs through the plastic hinge formation in two ends of beams. However, in the cable-cylinder bracing system, the cables provide stiffness for the system and avert the collapse mechanism.

When a low-stiffness cylinder is used, for example, PVC, if a lateral force imposes on the frame, the cables do not act for $\delta < \delta_s$, where δ is story displacement and δ_s is the specific story displacement at which the cable becomes linear and starts to act for greater displacements. δ_s is determined as follow:

$$\delta_s = \sqrt{(2l_{ext} + l_{int})^2 - h_c^2} - l_b \tag{1}$$

where h_c and l_b are the column height and beam length respectively. l_{ext} and l_{int} are:

$$l_{ext} = \sqrt{\left(\frac{l_b - l_p}{2}\right)^2 + \left(\frac{h_c - \phi_p}{2}\right)^2} \tag{2}$$

* Corresponding author. Faculty of Civil Engineering, K. N. Toosi University of Technology, No. 1346, Valiasr St., PO Box 15875, Tehran, Iran.
E-mail addresses: marziyeh.ghasemi.r@gmail.com (M. Ghasemi), fanaie@kntu.ac.ir (N. Fanaie), hossein.khorshidi@mail.kntu.ac.ir (H. Khorshidi).

https://doi.org/10.1016/j.jobe.2021.102309
Received 24 September 2020; Received in revised form 3 January 2021; Accepted 14 February 2021
Available online 20 February 2021

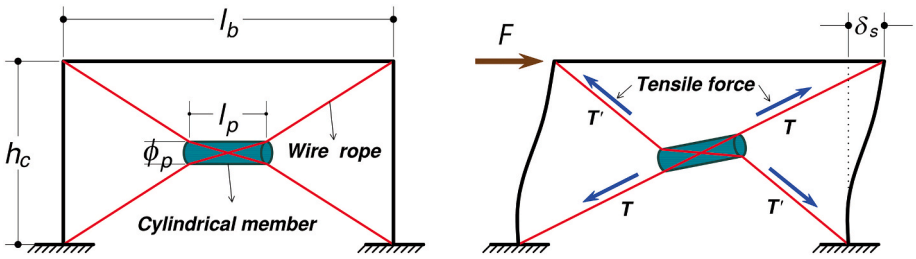

Fig. 1. Cable-cylinder bracing system: (a) concept, (b) deformation at $\delta = \delta_s$.

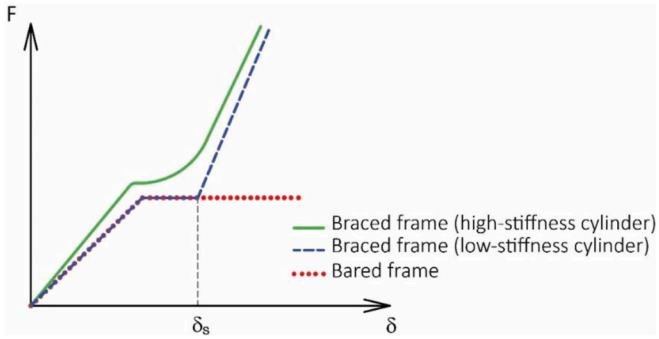

Fig. 2. The force-displacement relationship for the proposed bracing system.

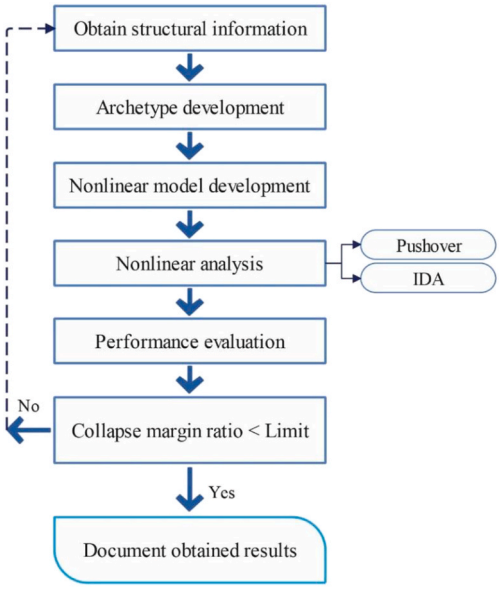

Fig. 3. The general framework of the FEMA P695 methodology [9].

Table 1
Performance group summary.

PG No.	Archetype ID	Design seismic load level	Period domain	Number of stories
PG-1	1	SDC C_{max}	short	2
PG-2	2		long	4
	3		long	6
	4		long	8
PG-3	5	SDC C_{min}	short	2
PG-4	6		long	4
	7		long	6
	8		long	8

$$l_{int} = \sqrt{l_p^2 + (\phi_p - \phi_B)^2} \tag{3}$$

where l_p and ϕ_p are the length and internal diameter of the cylindrical member respectively, and ϕ_B is the cable diameter.

In contrast, in the case of using a high-stiffness cylinder, for example steel, both cables perform in a story displacement lower than δ_s. Fig. 2 denotes the force-displacement relationship for the low and high-stiffness cylinder in the cable-cylinder systems.

In this method, the increase of the compression force of columns due to brace performance is prevented. Moreover, the lateral story strength is increased without decreasing the ductility of the MRF. Furthermore, it puts a limit on the lateral story displacement and thus prevents seismic energy concentration in a story. It has been proven that the proposed bracing system shows re-centering behavior. The results of seismic response analysis have indicated that because the cables do not act in the initial lateral displacements, the fundamental period of MRF and MRF with cable-cylinder braces are equal [4].

Hou and Tagawa [5] also studied the application of cable-cylinder bracing in a steel MRF with an elastoplastic damper. The proposed bracing system restrained story displacement within a specific range and has a re-centering effect on the frame.

Fanaie et al. [6] studied the theoretical performance of cable-cylinder bracing frames with a stiff cylinder. The stiffness of this system rises by increasing the frame lateral displacement. Moreover, the cables yield at larger displacement by raising the length and lowering the internal diameter of the cylindrical member. Two advantages of cable-cylinder bracing were presented over cross-cable bracing. Firstly, as the cables reach their ultimate strengths at larger frame lateral displacements, the frame ductility rises. Thus, the ductility drawback of the cable is solved. Secondly, in the most range of loading, both cables take tension force, so the cable impulse problem is removed.

Fanaie et al. [7] conducted another study to evaluate the behavior of the MRF with cable-cylinder bracing. By increasing the lateral displacement, the advantage of the cable-cylinder bracing system is more evident. Cable-cylinder bracing frames show higher energy dissipation compared to cable cross-bracing frames. Furthermore, cables and cylinders remain elastic during seismic events and do not have a role in energy dissipation. However, this system prevents the concentration of damage in a specific story by distributing the story displacement to the height of the structure. Moreover, the rise in the axial force of adjacent columns is lower in the cable-cylinder system in comparison with the cable cross-bracing frame. Their study confirmed that the needed cable area in the cable-cylinder bracing system is lower compared with that of in cable cross-bracing.

Fanaie and Zafari [8] performed the sensitivity analyses on the response modification factor of this system. Their study showed that the values of the over-strength factor, ductility factor, and response modification factor are higher for the cable-cylinder system in comparison to the cross-cable bracing system. Furthermore, in low pre-stressing stress, the response modification factor increases by raising the length and lowering the cylindrical member diameter. Moreover, the response modification factor decreases by increasing the pre-stressing stress of the cables. Also, the response modification factor is more sensitive to the

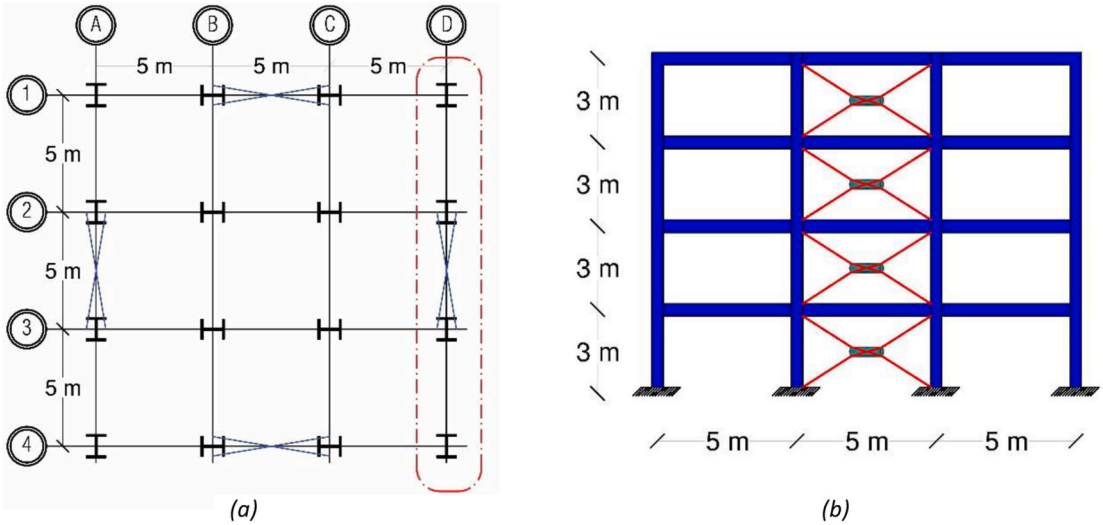

Fig. 4. Configuration of the studied structures: (a) plan view; (b) side view of the 4-story frame.

Table 2
Archetypes designed sections.

PG No.	Archetype ID	Story No.	Beam	Column		Cable area (mm^2)
				Exterior	Interior	
PG-1	1	1	W12X14	W8X15	W12X30	100
		2	W10X12	W8X15	W12X22	100
PG-2	2	1	W12X16	W12X26	W12X50	180
		2	W12X14	W12X22	W12X35	220
		3	W10X12	W12X19	W12X26	180
		4	W10X12	W12X19	W12X26	120
	3	1	W12X16	W10X26	W14X68	200
		2	W12X14	W10X26	W14X53	280
		3	W12X14	W10X22	W14X43	250
		4	W12X14	W10X22	W14X43	200
		5	W10X12	W10X19	W14X30	160
		6	W8X10	W10X19	W14X30	100
	4	1	W12X14	W10X30	W14X90	200
		2	W12X14	W10X30	W14X68	280
		3	W12X14	W10X30	W14X68	280
		4	W12X14	W10X30	W14X48	240
		5	W12X14	W10X26	W14X48	220
		6	W12X14	W10X26	W14X30	180
		7	W12X14	W10X19	W14X30	120
		8	W10X12	W10X19	W14X30	100
PG-3	5	1	W10X12	W10X15	W10X22	80
		2	W10X12	W10X15	W10X15	80
PG-4	6	1	W10X12	W12X22	W12X40	120
		2	W10X12	W12X22	W12X30	160
		3	W10X12	W12X16	W12X26	120
		4	W8X10	W12X14	W12X16	80
	7	1	W10X12	W10X26	W14X53	120
		2	W10X12	W10X26	W14X43	180
		3	W10X12	W10X22	W14X38	140
		4	W10X12	W10X22	W14X38	120
		5	W10X12	W10X15	W14X26	100
		6	W8X10	W10X15	W14X22	80
	8	1	W10X12	W10X30	W14X68	140
		2	W10X12	W10X30	W14X61	200
		3	W10X12	W10X26	W14X48	180
		4	W10X12	W10X26	W14X48	180
		5	W10X12	W10X22	W14X34	140
		6	W10X12	W10X22	W14X34	120
		7	W10X12	W10X17	W14X30	100
		8	W8X10	W10X17	W14X30	80

pre-stressing of cables in comparison to the size of the cylindrical member.

As the Seismic Performance Factors (SPFs) of the cable-cylinder bracing system are not established in current seismic building codes, this paper aims to quantify the SPFs including the response modification factor (R), the over-strength factor (Ω_0), and the deflection amplification factor (C_d) for such systems as an innovative displacement-restraint bracing method. FEMA P695 [9] describes a methodology to quantify the structural performance and determine the SPFs of new seismic-force-resisting systems for use in seismic design. Several studies have been performed to assess the seismic performance of various structural systems according to FEMA P695 methodology [10–13]. In this investigation, eight frame models equipped with cable-cylinder braces with high-stiffness cylinder (like a steel cylinder) of 2-, 4-, 6-, and 8-story buildings were designed with presumed SPFs. The numerical models of the structures were simulated using OpenSees software [14] and considering lump plasticity to capture cyclic strength and stiffness deterioration caused by structural damage. To provide insight into the collapse performance of this system, nonlinear static analysis (pushover) and Incremental Dynamic Analysis (IDA) were conducted using a set of 44 ground motion records. Finally, the performance of the intended system was assessed as per FEMA P695 procedure [9].

2. General framework

The FEMA P695 methodology [9] introduces a framework to evaluate the SPFs of new structural systems and also to assess the collapse risk of structures. To use this approach, it is needed to apply valid ground motions on representative nonlinear models that require design information and nonlinear test data. This technical approach considers the uncertainties in test data, design, modeling, and ground motion.

The methodology comprised of the following major steps:

- Obtain required information, consisting of the design requirements details, criteria, and results from experimental studies. This information will be used in nonlinear model development and also to consider uncertainties.
- Characterize the behavior of the system by developing structural archetypes. Archetypes are seismic-resisting systems to representative configuration and other important features of the proposed system.
- Develop structural nonlinear models for collapse assessment. Models are calibrated using experimental data to simulate expected nonlinear behavior.

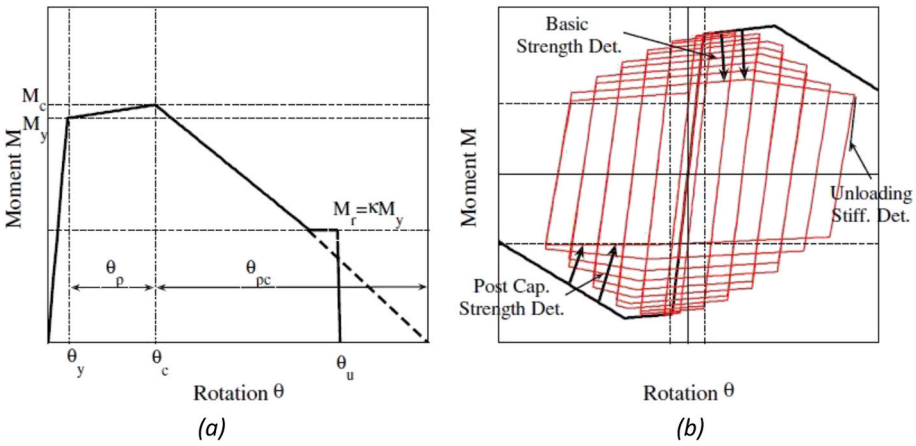

Fig. 5. Modified IK deterioration model: (a) monotonic curve; (b) the cyclic determination and associated definitions [20].

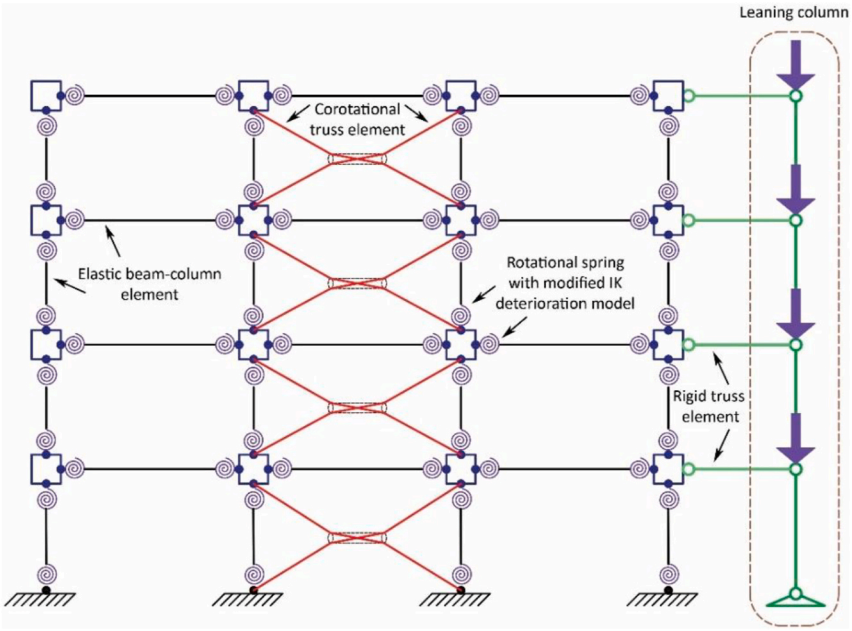

Fig. 6. 2D frame modeling approach in OpenSees.

- Conduct nonlinear static analysis (pushover) and Incremental Dynamic Analysis (IDA) to assess collapse behavior. The primary purpose of nonlinear static analyses is to confirm the general performance of nonlinear models and to evaluate the over-strength factor and ductility factor of the frames. Incremental dynamic analyses are also conducted to determine median collapse capacities, collapse margin ratios, and fragility curves.
- Performance evaluation by using nonlinear analyses data to establish the value of the system over-strength factor (Ω_0), and to assess the acceptability of the initial value of the response modification factor, R. Moreover, the deflection amplification factor, C_d, is determined by considering an acceptable value of R, and the effective damping of the system.

Fig. 3 illustrates the general framework of the FEMA P695 procedure.

3. Archetypes development

To generalize the predictions of system behavior, FEMA P695 [9] presents a procedure to select a group of buildings named "archetypes". Archetypes are representations of a seismic resisting system that represent the behavior of a structure. So, the archetypes are divided into different Performance Groups (PGs) to consider key contrasts in configuration, gravity and seismic load levels, and period domain of the system.

In this study, one basic structural configuration, constant gravity loads, two design seismic load levels, and two period domains resulted in four PGs as shown in Table 1.

Eight frame models have been applied in this research by defining 2-, 4-, 6-, and 8-story frames. In all models, the height of stories and the length of bays in each direction were assumed to be 3 m and 5 m respectively.

Fig. 4 illustrates the elevation of a 4-story frame and the typical plan of archetypes as well as the location of the cable-cylinder braces in the frames.

Archetypes with Intermediate Moment Resisting Frame (IMRF) and cable-bracing system were designed using the equivalent lateral force approach proposed in section 12.8 of ASCE/SEI 7–16 [15]. The design criteria of AISC 360–16 [16] and the seismic provisions suggested by AISC 341–16 [17] were also applied to design the steel members. The designed archetypes were finally checked for the maximum allowable story drift per ASCE/SEI 7–16 [15].

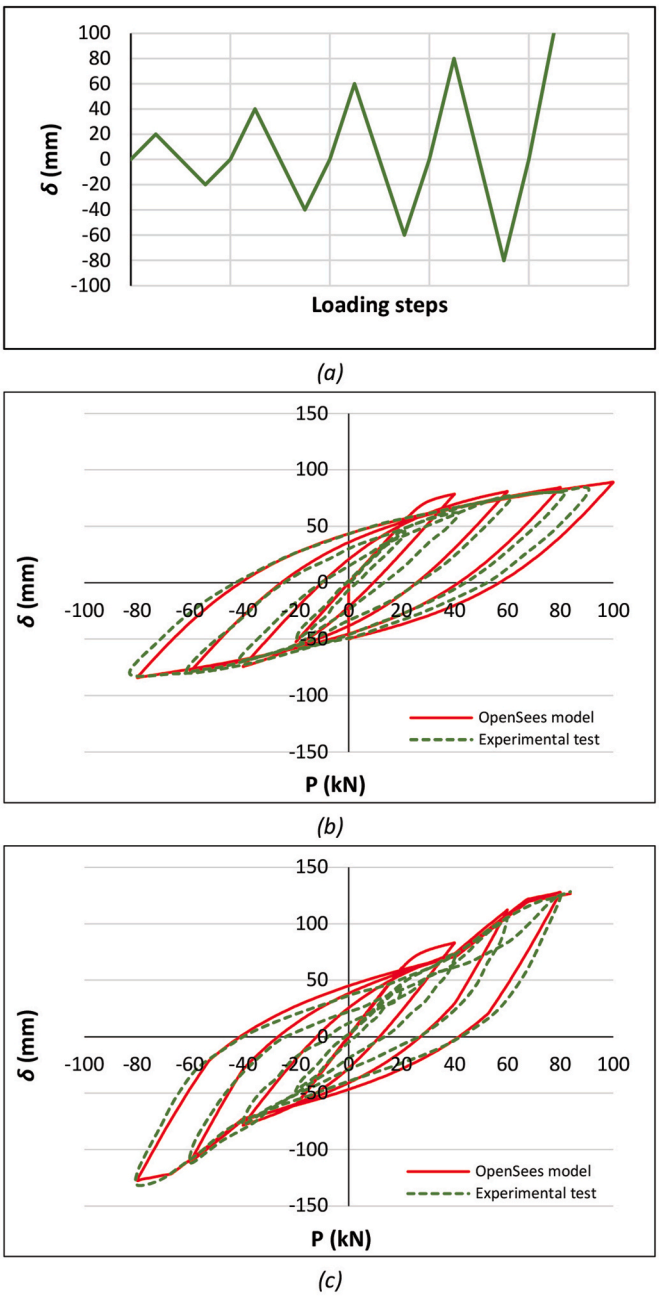

Fig. 7. The experimental and the numerical response: (a) loading protocol; (b) MRF; (c) MRF with cable-cylinder bracing system.

The steel material for all beam and column members was assumed to be ST37 with the modulus of elasticity of 200 GPa and the yield strength of 240 MPa. The material property of the cables was presumed to be Grade 270 steel with the modulus of elasticity of 160 GPa and the yield strength of 1600 MPa, based on ASTM A416 [18].

Gravitational dead and live loads on each floor were supposed to be 6 and 2 kN/m^2 respectively. The corresponding values were 6.65 kN/m^2 and 1.5 kN/m^2 for the roof floor. The cladding load of 1.25 kN/m^2 was also assumed on each floor level. Dead load and 20% of the live load of the frames were applied to base an estimate on the seismic mass. Considering no irregularity in both elevation and plan, all diaphragms have been considered as rigid.

The spectral intensities corresponding to the Seismic Design Category (SDC) C are considered per FEMA P695 methodology [9]. So, the archetypes were designed for SDC C_{max} and C_{min} ground motions. Since

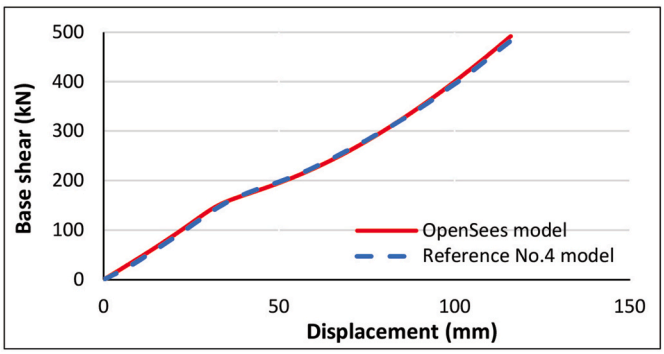

Fig. 8. Pushover curves of the OpenSees model and study conducted by Hou and Tagawa [4].

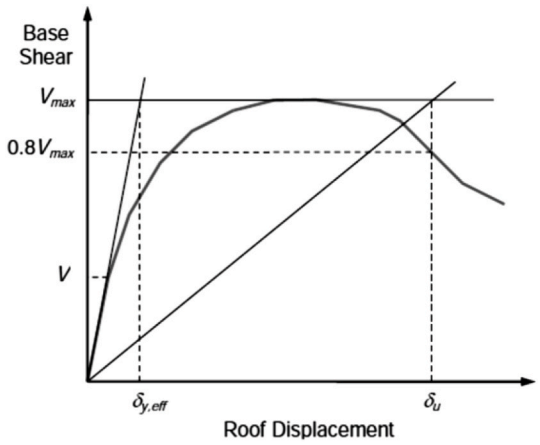

Fig. 9. Idealized pushover curve.

seismic design codes do not consider the cable-cylinder frames as one of the seismic-force-resisting systems, the criteria of Ordinary Concentric Braced Frames (OCBFs) were employed in lieu of cable-cylinder bracing frames to ensure the possible application of the proposed system. Accordingly, higher intensities were not investigated, due to the ASCE/SEI 7–16 recommendation [15] that limits the application of OCBFs in SDC D. The Maximum Considered Earthquake (MCE), 5% damped spectral response acceleration parameter at short periods, and at a period of 1 s adjusted after site class effects, S_{MS} and S_{M1}, were considered as 0.75g and 0.3g respectively for SDC C_{max}. These parameters were assumed as 0.5g and 0.2g respectively for SDC C_{min}.

The needed SPFs to determine the equivalent lateral force were presumed initially. Based on the previous relevant study [8], the trial value of the R factor was initially presumed equal to 4 for this system. A value of 2.5 was also assumed for the over-strength factor. The deflection amplification factor (C_d) is supposed to be equal to the R factor as proposed by FEMA P695 [9].

The design results of the archetypes are depicted in Table 2. The length and diameter of the cylinder were, respectively, 700 mm and 200 mm for all archetypes.

4. Nonlinear model development

In this research, OpenSees software ver.3.0.3 [14] was used to develop 2D nonlinear Finite Element (FE) models.

The beams and columns were simulated adopting an elasticBeamColumn element and zeroLength elements with rotational springs at the ends of the member. The modified Ibarra-Krawinkler (Bilin material) model with the bilinear hysteretic response was used to capture the nonlinear behavior of the rotational springs in plastic

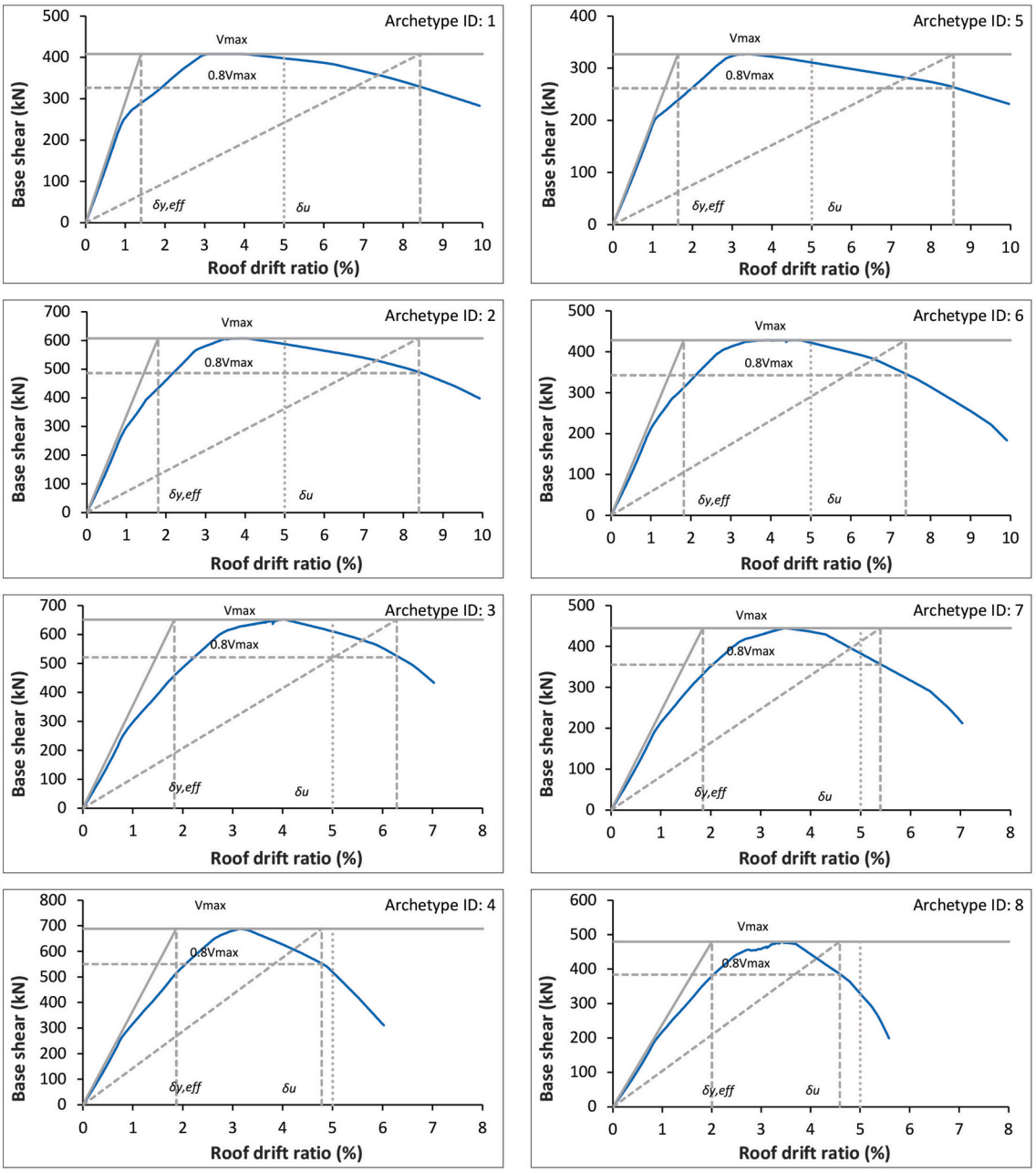

Fig. 10. Pushover results of the archetypes.

Table 3
Summary of pushover analyses of the archetypes.

PG No.	Archetype ID	V_{max} (kN)	V (kN)	Ω	$\delta_{y,eff}$ (%)	μ_T
PG-1	1	408.23	165.68	2.46	1.40	3.58
	Average Ω			2.46		
PG-2	2	607.68	276.09	2.20	1.80	2.78
	3	651.55	303.17	2.15	1.83	2.73
	4	688.78	325.94	2.11	1.87	2.56
	Average Ω			2.15		
PG-3	5	326.91	109.86	2.98	1.64	3.06
	Average Ω			2.98		
PG-4	6	428.33	168.98	2.53	1.82	2.75
	7	444.61	186.23	2.39	1.84	2.72
	8	480.00	201.36	2.38	2.00	2.29
	Average Ω			2.43		

hinges. This technique takes the cyclic strength and stiffness deterioration caused by structural damage into account. As shown in Fig. 5, the mentioned model is determined by the following main parameters: strength parameters (M_y: the effective yield strength, M_c: the capping strength, M_r: the residual strength); deformation parameters (θ_y: the effective yield rotation, θ_p: the pre-capping rotation capacity for monotonic loading, θ_{pc}: the post-capping rotation capacity, θ_u: the ultimate rotation capacity); K_e: effective stiffness; and κ: cyclic deterioration parameter. The relevant parameters were selected based on the extensive experimental studies [19,20].

The method proposed by ATC 72–1 [21] was used to simulate the panel zones. According to the study conducted by Gupta and Krawinkler [22], to model the shear distortion hysteretic behavior of the panel zones of the beam to column connections a trilinear behavior was used.

The effect of P-delta caused by gravity loads was considered by using leaning columns. The leaning columns adopt large cross-areas and are linked to each floor level of the main structure by using rigid truss

Table 4
Summary of the far-field record set data [9].

NO.	Event name	Year	M	Fault type	PGA_{max} (g)	PGV_{max} (cm/s)
1	Northridge	1994	6.7	thrust	0.52	63
2	Northridge	1994	6.7	thrust	0.48	45
3	Duzce, Turkey	1999	7.1	Strike-Slip	0.82	62
4	Hector Mine	1999	7.1	Strike-Slip	0.34	42
5	Imperial Valley	1979	6.5	Strike-Slip	0.35	33
6	Imperial Valley	1979	6.5	Strike-Slip	0.38	42
7	Kobe, Japan	1995	6.9	Strike-Slip	0.51	37
8	Kobe, Japan	1995	6.9	Strike-Slip	0.24	38
9	Kocaeli, Turkey	1999	7.5	Strike-Slip	0.36	59
10	Kocaeli, Turkey	1999	7.5	Strike-Slip	0.22	40
11	Landers	1992	7.3	Strike-Slip	0.24	52
12	Landers	1992	7.3	Strike-Slip	0.42	42
13	Loma Prieta	1989	6.9	Strike-Slip	0.53	35
14	Loma Prieta	1989	6.9	Strike-Slip	0.56	45
15	Manjil, Iran	1990	7.4	Strike-Slip	0.51	54
16	Superstition Hills	1987	6.5	Strike-Slip	0.36	46
17	Superstition Hills	1987	6.5	Strike-Slip	0.45	36
18	Cape Mendocino	1992	7	thrust	0.55	44
19	Chi-Chi, Taiwan	1999	7.6	thrust	0.44	115
20	Chi-Chi, Taiwan	1999	7.6	thrust	0.51	39
21	San Fernando	1971	6.6	thrust	0.21	19
22	Friuli, Italy	1976	6.5	thrust	0.35	31

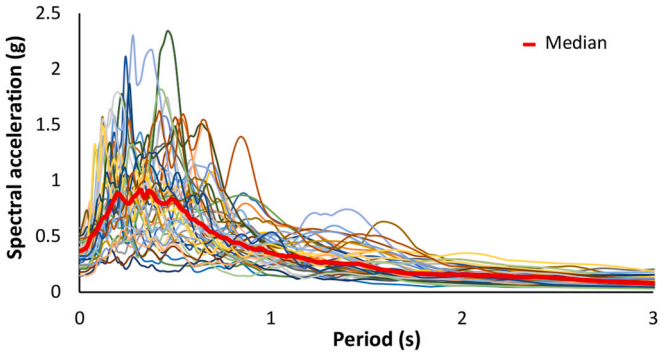

Fig. 11. Spectra of normalized far-field ground motions.

elements.

To stimulate the hysteretic behavior of cable-cylinder braces, the Elastic-Perfectly Plastic Gap material as well as the corotational truss element were adopted. Fig. 6 shows the modeling details followed in this study.

The story masses were concentrated at the floor nodes. To consider the rigid floor, equalDOF command was used to constraint all nodes in each story level. Additionally, in the numerical model, a Rayleigh damping of 5% for the first and the second modes was considered.

To verify the accuracy of the modeling, two MRFs with and without the cable-cylinder bracing system under cyclic loading based on experiments performed by Hou and Tagawa [4] were simulated in OpenSees software. The steel columns and beam of H 150*150*7*10 were assumed to be made from SN400B grade. The 10 mm-diameter cables were also presumed to be 7*19 stainless steel strand (SUS316) with yield load and ultimate load of 57.9 kN and 60.2 kN respectively. The length and inner diameter of the cylinder were considered to be 214 mm and 40 mm respectively. Hysteretic responses of experimental and numerical models are shown in Fig. 7.

Moreover, a two-dimensional frame with one story and one bay was also considered from the numerical study conducted by Hou and Tagawa [4]. The story height and span length were considered 3.5 m and 5 m respectively. The rigid beam and columns with a box section of 200 mm depth and width and 8 mm thickness were assumed. The outer diameter of cables was considered to be 28 mm, and the dimensions of the cylinder were selected to result in $\delta_s = 58$ mm based on Eq. (1). Nonlinear static analyses were performed and the pushover curves are presented in Fig. 8.

As depicted in Figs. 7 and 8 the modeling in OpenSees coincides with the relevant study [4], which verifies assumptions in geometric, materials, sections, and elements.

In accordance with FEMA P695 [9], if it is impossible to simulate all deterioration modes which lead to the collapse of the structure, non-simulated collapse modes are alternative limits for the structural response. Simulated collapse modes were modeled considering the nonlinear behavior of structural members. However, non-simulated collapse modes of cable-cylinder bracing systems are not noted, as only limited experimental and analytical research has been done on these bracing systems. An experimental study conducted by Hou and Tagawa [4] indicated that the collapse mode of the cable-cylinder system occurs at a drift ratio of nearly 5%. Consequently, in this study, the non-simulated collapse limit state was assumed as the state in which the story drift ratio reaches 5%.

5. Nonlinear analyses

5.1. Nonlinear static analyses (pushover)

Nonlinear static analyses are conducted to confirm the nonlinear behavior of the model and to evaluate the over-strength factor (Ω) and period-based ductility factor (μ_T) of archetypes. Generally, pushover analyses are performed using the procedure proposed in ASCE/SEI 41–17 [23]. The gravity load for pushover analyses is given by the following load combination, per FEMA P695 [9]:

$$1.05D + 0.25L \tag{4}$$

where D is the total dead load of the structure, and L is the live load.

Moreover, the vertical distribution of the lateral force, F_x, at each floor level, x, is considered as follows:

$$F_x \propto m_x \phi_{1,x} \tag{5}$$

where m_x is the mass at level x; and $\phi_{1,x}$ is the ordinate of the fundamental mode at level x.

According to Fig. 9 and considering FEMA P695 methodology [9], the over-strength factor, Ω, is determined as the ratio of the maximum base shear capacity (V_{max}) to the design base shear (V):

$$\Omega = \frac{V_{max}}{V} \tag{6}$$

The period-based ductility factor, μ_T, is determined as the ratio of ultimate roof displacement, δ_u, to the effective yield roof displacement, $\delta_{y,eff}$:

$$\mu_T = \frac{\delta_u}{\delta_{y,eff}} \tag{7}$$

The effective yield roof displacement is determined by Eq. (8):

$$\delta_{y,eff} = C_0 \frac{V_{max}}{W} \left[\frac{g}{4\pi^2}\right] (\max(T, T_1))^2 \tag{8}$$

where C_0 is a function of fundamental mode displacement and roof displacement, V_{max} is the maximum base shear, W is the structure weight, and g is the gravity constant.

The coefficient C_0 is computed using Eq. (9), as follows:

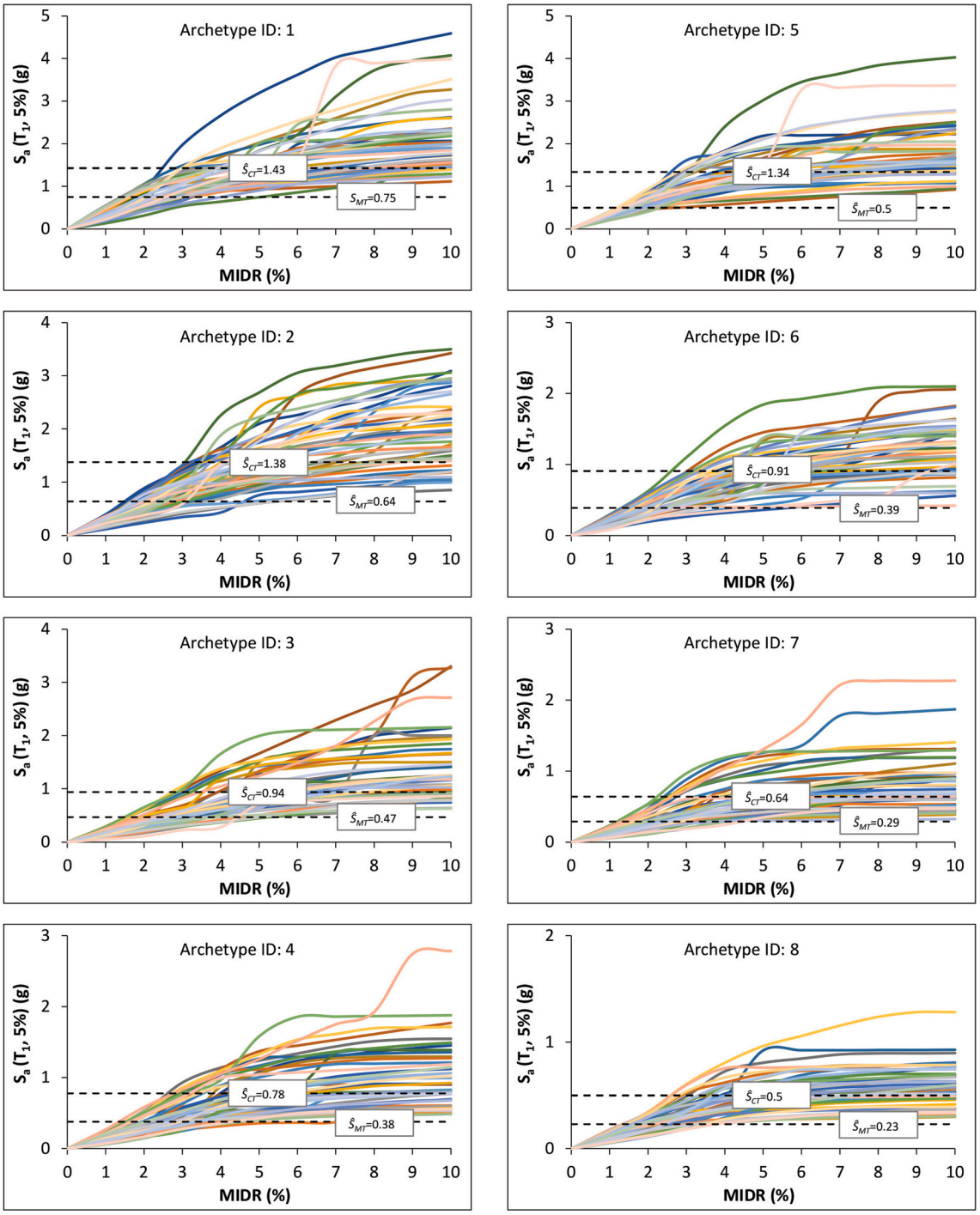

Fig. 12. IDA results of the archetypes.

$$C_0 = \phi_{1,r}\frac{\sum_1^N m_x\phi_{1,x}}{\sum_1^N m_x\phi_{1,x}{}^2} \tag{9}$$

where m_x is the mass at floor x, and $\phi_{1,x}$ ($\phi_{1,r}$) is the ordinate of the fundamental mode at floor x (roof), and N is the total number of levels.

Finally, T is the fundamental period defined by Eq. (10), and T_1 is the fundamental period of the frame obtained from eigenvalue analysis.

$$T = C_u T_a = C_u C_t h_n^x \tag{10}$$

where h_n is the structure height, the values of the coefficient, C_u, C_t, and x are presented in Tables 12.8–1 and 12.8–2 of ASCE/SEI 7–16 [15].

According to FEMA P695 [9], in this study, the ultimate roof displacement, δ_u in the pushover curve, was considered as the roof displacement associated with a 20% loss of V_{max} or the occurrence of the non-simulated collapse mode, whichever occurs first.

The pushover curves from nonlinear static analyses are illustrated in Fig. 10, and the values are summarized in Table 3.

It could be observed that as a general trend, the value of the over-strength factor and the period-based ductility factor declined by raising the height of the archetypes.

It should be noted that there is a sharp fall in the pushover curves of

Table 5
Summary of nonlinear dynamic analyses of the archetypes.

PG No.	Archetype ID	$\hat{S}_{CT}$	T (s)	S_{MT} (g)	CMR
PG-1	1	1.43	0.28	0.75	1.91
PG-2	2	1.38	0.47	0.64	2.17
	3	0.94	0.64	0.47	2.00
	4	0.78	0.79	0.38	2.07
PG-3	5	1.34	0.31	0.5	2.67
PG-4	6	0.91	0.51	0.39	2.33
	7	0.64	0.70	0.29	2.23
	8	0.50	0.86	0.23	2.15

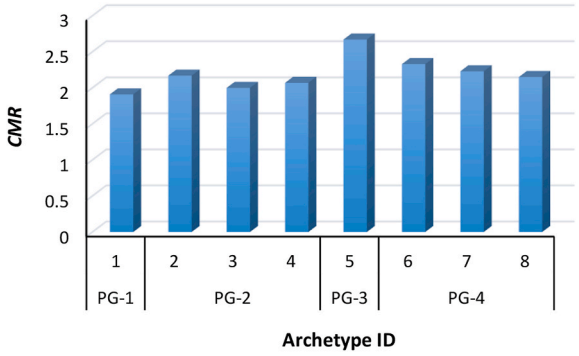

Fig. 13. Comparison of the CMR value of the archetypes.

the 6- and 8-story frames, which validates the fact that the cable-cylinder bracing system is an improper method to improve the seismic behavior of taller frames.

5.2. Incremental Dynamic Analysis (IDA)

Nonlinear dynamic analyses are conducted to establish median collapse capacity, $\hat{S}_{CT}$, and Collapse Margin Ratios (CMR) which describes the collapse safety of each archetype and will be discussed in this section.

According to FEMA P695 [9], two groups of ground motion records are presented for performing IDA. One set represents far-field set and is comprised of 22 pairs of ground motion records from the sites at a distance of more than or equal to 10 km from fault rupture. On the other hand, the near-field set is made up of 28 pairs of ground motions recorded at sites less than 10 km from fault rupture. Whilst both far-field and near-field record groups are presented in this provision, only the far-field records are required for collapse evaluation. Table 4 presents a summary of ground motion records utilized in IDA. The larger value of Peak Ground Acceleration (PGA) and Peak Ground Velocity (PGV) of the two components for each record is reported as PGA_{max} and PGV_{max}.

The ground motion records had been scaled taking a two-steps approach before being used in IDA according to FEMA P695 methodology [9]. Firstly, individual records were normalized by their PGV to eliminate unwarranted variability in ground motion records, without omitting overall variability. Secondly, normalized records in the previous stage were scaled to a certain ground motion intensity such that the median spectral acceleration of the record set matches the spectral acceleration at the fundamental period, T, of each archetype model. The acceleration spectra of far-field ground motion records and the median response spectrum are illustrated in Fig. 11.

For plotting the IDA outputs, the Damage Measure (DM) was considered to be the Maximum Inter-story Drift Ratio (MIDR), whilst the Intensity Measure (IM) was assumed to be spectral acceleration based on the site 5% damped design spectra at the fundamental period of the building, S_a (T_1, 5%). The gravity loads are the same as those used for pushover analysis and described in Eq. (4).

Median collapse capacity ($\hat{S}_{CT}$) is determined as the ground motion intensity in which 50% of the total records contribute to structural collapse.

The Collapse Margin Ratio (CMR) is the ratio of the median collapse capacity ($\hat{S}_{CT}$) to the MCE spectral intensity at the fundamental period of the frame (S_{MT}). Indeed, it indicates the safety margin of a structure against collapse in an earthquake. CMR was computed using Eq. (11):

$$CMR = \frac{\hat{S}_{CT}}{S_{MT}} \tag{11}$$

where MCE intensity (S_{MT}) could be determined from the MCE design spectrum proposed by FEMA P695 [9] for different SDCs.

The obtained results are presented in Fig. 12, and the values are summarized in Table 5 and Fig. 13.

The results confirm that the archetypes designed in low SDC (C_{min}) have higher $CMRs$ than those designed in high SDC (C_{max}). Moreover, since the IDA curves level off at nearly 5% drift, selecting such a drift as a limit for occurrence of the archetype collapse is reasonable for collapse assessment.

To consider the influence of spectral shape, the CMR is adapted to Adjusted Collapse Margin Ratio ($ACMR$) for each archetype model, i, as defined in Eq. (12):

$$ACMR_i = CMR_i \times SSF_i \tag{12}$$

where SSF (Spectral Shape Factor) is a function of the fundamental period (T), μ_T, and SDC.

Moreover, it is important to consider the effect of considerable uncertainty sources that could cause variable collapse capacities. The record-to-record uncertainty (RTR); design requirements uncertainty (DR); test data uncertainty (TD); and modeling uncertainty (MDL) were taken into account in the collapse assessment process. These parameters depend on certain factors, such as technical knowledge and the capacity for simulating the behavior of the structural system. The total uncertainty is computed by Eq. (13):

$$\beta_{tot} = \sqrt{\beta_{RTR}^2 + \beta_{DR}^2 + \beta_{TD}^2 + \beta_{MDL}^2} \tag{13}$$

where β_{tot} is the system collapse uncertainty. β_{RTR}, β_{DR}, β_{TD}, and β_{MDL} are collapse uncertainties corresponding to record-to-record, design requirements, test data, and modeling respectively. For systems with $\mu_T < 3$, the value of β_{RTR} can be calculated by Eq. (14):

$$\beta_{RTR} = 0.1 + 0.1\mu_T \tag{14}$$

where β_{RTR} must be greater than or equal to 0.20.

The design requirement uncertainty (β_{DR}) represents the completeness and robustness of the design requirements and confidence in the basis for the design equations. The latest editions of design codes with reasonable safeguards against unanticipated failure modes were used in this research, and most of the important design and quality assurance requirements were specified but did not fully address all the aspects of fabrication, erection, and final construction. On the other hand, conventional materials with specified properties were used in this study. Therefore, the quality of the design requirements was good (B), and the quantitative value of $\beta_{DR} = 0.2$ was assigned.

The test data uncertainty (β_{TD}) is related to the comprehensiveness and robustness of the test data used to assess the behavior of the proposed seismic-force-resisting system. The quality rating depends not only on the quality of the testing program but also on how well the tests address key parameters and behavioral issues. Nearly all behavior aspects of the system are generally understood, and the test results are supported by basic principles of mechanics. Therefore, test data uncertainty was supposed to be good (B), and the corresponding value was $\beta_{TD} = 0.2$.

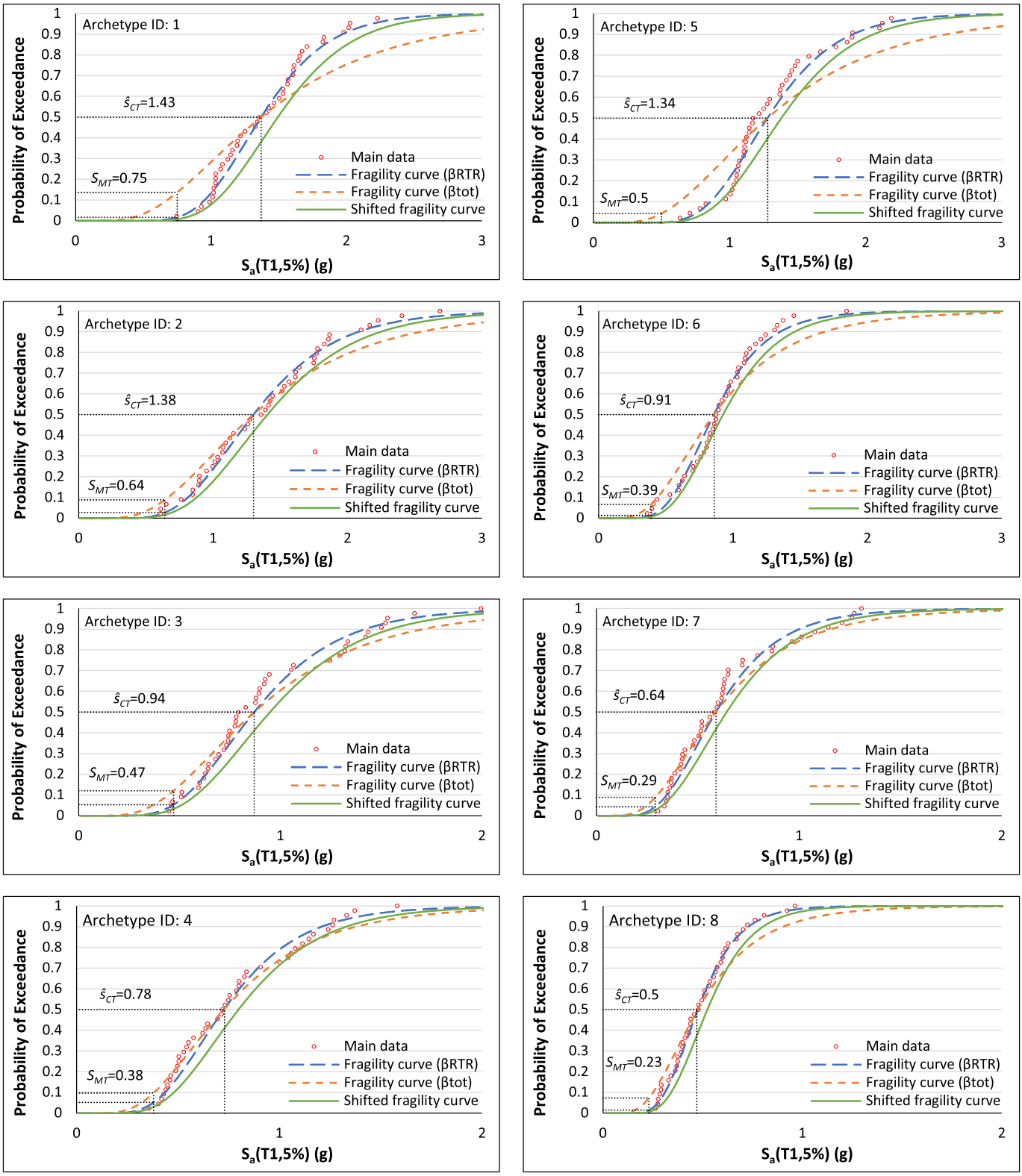

Fig. 14. Fragility curves of the archetypes.

The modeling uncertainty indicates how well the numerical models represent the range of structural collapse characteristics and associated design parameters, and also how well the analysis models capture structural collapse behavior through both direct simulation and non-simulated limit state checks. In this study, the analytical models were developed to consider the deterioration behavior of the components, and the parameters of nonlinear models have been well-calibrated based on the experimental results. Based on these ratings, the quality of the numerical model was considered good (B), and the value of $\beta_{MDL} = 0.2$ was used.

Acceptable values of *ACMR* are obtained according to β_{tot} and probabilities of collapse. As per FEMA P695 [9], acceptable performance

is accomplished if the average value of *ACMR* for each PG meets $ACMR_{10\%}$ criteria, and individual values of *ACMR* for each archetype in a PG exceeds $ACMR_{20\%}$, as shown in Eqs. (15) and (16):

$$\overline{ACMR_i} \geq ACMR_{10\%} \tag{15}$$

$$ACMR_i \geq ACMR_{20\%} \tag{16}$$

The relation between the ground motion intensity and the probability of the structure collapse could be shown on the fragility curve. It is plotted considering a Cumulative Distribution Function (CDF) from IDA results. The lognormal collapse fragility is determined by two main factors: the median collapse intensity ($\hat{S}_{CT}$) and the standard deviation of the natural logarithm.

Fig. 14 illustrates three groups of collapse fragility curves acquired by applying a lognormal distribution to the collapse points of IDA curves. Two dashed fragility curves were determined considering β_{RTR} and β_{tot} as the standard deviation parameter in the lognormal cumulative distributive function, and the solid curve (shifted fragility curve) was drawn by multiplying the fragility curve with β_{RTR} by *SSF*.

As shown in Fig. 14, considering additional uncertainty leads to a reduction in the slope of the fragility curve and increases the probability of structure collapse at the MCE intensity (S_{MT}). Indeed, by considering additional uncertainty for the system, a larger collapse margin ratio is needed.

6. Evaluation of Seismic Performance Factors (SPFs)

As mentioned in previous sections, an initial response modification factor, *R*, was assumed to design the archetypes. In this stage, the acceptability of the trial value of *R* is assessed per FEMA P695 methodology [9]. Acceptability means comparing the *ACMR* with acceptable values as presented in Eqs. (15) and (16) in the previous section.

Based on Fig. 3, if the SPFs of the archetypes could not be passed, the system should be reanalyzed and redesigned, and the performance evaluation steps should be repeated.

As presented in Table 6, both the criteria were satisfied for all individual archetypes and all PGs. As a result, the value of R factor 4 ensures safety against collapse in the seismic event and is appropriate for these lateral load resisting systems.

Though the average *ACMR* is close to the $ACMR_{10\%}$ for PG-1, for the other cases the values of *ACMR*s are significantly above the acceptable values. Furthermore, the largest *ACMR* occurs for PG-3 that is a frame with a considerable over-strength factor. It could be due to the dominance of gravity loads in designing the archetypes, particularly when seismic design loads are low in comparison with the gravity loads.

The value of the system over-strength factor, Ω_0, should be taken as more than the largest average value of computed archetype over-strength factor for each PG and also should be rounded to half unit intervals. As proposed by FEMA P695 [9], the system final over-strength factor should be restricted to 3. Consequently, as shown in Table 3, the maximum average of the over-strength factor has a value of 2.98, so the system over-strength factor was supposed to be equal to 3.

Finally, as given in Eq. (17), the deflection amplification factor, C_d, is determined as the ratio of response modification factor, *R*, to the damping coefficient, B_I, corresponding to the effective damping of the system:

$$C_d = \frac{R}{B_I} \tag{17}$$

As presented in Table 7, as the effective damping of the system, β_I, was presumed to be 5% of critical, the B_I coefficient, is equal to 1.0, according to ASCE/SEI 07–16 [15]. Thus, the value of C_d will be equal to the value of *R*.

Table 6
Summary of ACMRs and comparison to acceptable criteria.

PG No.	Archetype ID	*SSF*	*ACMR*	$ACMR_{20\%}$	$ACMR_{10\%}$	Pass/Fail
PG-1	1	1.09	2.07	1.59		**Pass**
	Average		2.07		2.02	**Pass**
PG-2	2	1.08	2.33	1.56		**Pass**
	3	1.09	2.18	1.56		**Pass**
	4	1.10	2.27	1.52		**Pass**
	Average		2.26		1.96	**Pass**
PG-3	5	1.08	2.89	1.59		**Pass**
	Average		2.89		2.02	**Pass**
PG-4	6	1.08	2.51	1.56		**Pass**
	7	1.09	2.44	1.56		**Pass**
	8	1.10	2.36	1.52		**Pass**
	Average		2.44		1.96	**Pass**

Table 7
Damping coefficient [15].

Effective damping (β_I)	Damping coefficient (B_I)
≤2	0.8
5	1
10	1.2
20	1.5
30	1.8
40	2.1
50	2.4
60	2.7
70	3
80	3.3
90	3.6
100	4

7. Conclusion

Cable-cylinder bracing system is a modern alternative to design structures or retrofit the existing buildings. In this study, seismic performance evaluations were performed for 2, 4, 6, and 8-story cable-cylinder braced steel frames, according to the procedure proposed by FEMA P695. The nonlinear static analyses (pushover) were conducted to assess the over-strength factor (Ω) and period-based ductility factor (μ_T) of the intended archetypes. In the next step, by conducting nonlinear Incremental Dynamic Analysis (IDA), the safety margin ratio against collapse was determined for each archetype. Finally, the acceptability of assumed Seismic Performance Factors (SPFs) were controlled based on the estimated total system uncertainty of the archetype frames.

The results obtained from pushover analyses indicate that the over-strength factor (Ω) and the period-based ductility factor (μ_T) of the archetypes declined by rising the structure height. Moreover, the IDA results show that the IMRFs with cable-cylinder bracing designed in low Seismic Design Category (SDC) have higher *CMR*s than those designed in high SDC. The fragility curves depict that considering additional uncertainty leads to a reduction in the slope of the fragility curve and increases the probability of collapse at the MCE intensity (S_{MT}). In other words, by considering additional uncertainty, a larger Collapse Margin Ratio (*CMR*) is needed for the structure. Furthermore, the largest *ACMR* occurs for the frame with a considerable over-strength factor. It could be due to the dominance of gravity loads in designing the archetypes, particularly when seismic design loads are low in comparison with the gravity loads. The computed *ACMRs* for each individual archetype and each Performance Group (PG) satisfied the limits of FEMA P695. Thus, the results of performance evaluation indicate that an R = 4, $\Omega_0 = 3$, and $C_d = 4$ are appropriate to design the dual systems with IMRF and cable-cylinder bracing as per FEMA P695.

To the best knowledge of the authors, these new braces are under study and have not been used in new buildings yet. From a practical

viewpoint, the substantial seismic lateral force in tall buildings results in a considerable needed cross-sectional area for the cables. Thus, this system is not practical in high-rise structures with one braced bay. In spite of the efforts to cover a wide range of archetypes, the proposed SPFs are valid for the assumed parameters in this study. Changes in the basic structural configuration should be considered in further studies to capture major variations in the seismic force-resisting system that may influence the structural response. Variations in the distribution of braced bays, permitted vertical irregularities, beam spans, and the number of bays are examples of alternative configurations.

CRediT authorship contribution statement

Marziyeh Ghasemi: Investigation, Software, Writing – original draft. **Nader Fanaie:** Conceptualization, Methodology, Supervision, Validation. **Hossein Khorshidi:** Data curation, Visualization, writing reviewing and editing.

Declaration of competing interest

The authors declare that they have no known competing financial interests or personal relationships that could have appeared to influence the work reported in this paper.

Acknowledgments

This research did not receive any specific grant from funding agencies in the public, commercial, or not-for-profit sectors.

References

[1] S. Costanzo, M. D'Aniello, R. Landolfo, Proposal of design rules for ductile X-CBFS in the framework of EUROCODE 8, Journal of Earthquake Engineering and Structural Dynamics (2018) 1–28, https://doi.org/10.1002/eqe.3128.
[2] A. Longo, R. Montuori, V. Piluso, Failure mode control of X-braced frames under seismic actions (2008), J. Earthq. Eng. 12 (5) (2008) 728–759, https://doi.org/10.1080/13632460701572955.
[3] S. Costanzo, M. D'Aniello, R. Landolfo, A. De Martino, Critical discussion on seismic design criteria for cross concentrically braced frames, Ingegneria Sismica 35 (2) (2018) 23–36.
[4] X. Hou, H. Tagawa, Displacement-restraint bracing for seismic retrofit of steel moment frames, J. Constr. Steel Res. 65 (2009) 1096–1104. https://doi:10.1016/j.jcsr.2008.11.008.
[5] X. Hou, H. Tagawa, Wire-rope bracing system with elasto-plastic dampers for seismic response reduction of steel frames, in: The 14th World Conference on Earthquake Engineering, 2008.
[6] N. Fanaie, S. Aghajani, E. Afsar Dizaj, Theoretical assessment of the behavior of cable bracing system with central steel cylinder, Adv. Struct. Eng. 19 (3) (2016) 463–472, https://doi.org/10.1177/1369433216630052.
[7] N. Fanaie, S. Aghajani, E. Afsar Dizaj, Strengthening of moment resisting frame using cable-cylinder bracing, Adv. Struct. Eng. (2016) 1–19. https://doi:10.1177/1369433216649382.
[8] N. Fanaie, N. Zafari, Sensitivity analysis on response modification factor of new cable-cylinder bracing systems, J. Earthq. Eng. (2017), https://doi.org/10.1080/13632469.2017.1326419.
[9] Federal Emergency Management Agency, NEHRP Quantification of Building Seismic Performance Factors (FEMA P 695), Washington, D.C, 2009.
[10] M. Yakhchalian, N. Asgarkhani, M. Yakhchalian, Evaluation of deflection amplification factor for steel buckling restrained braced frame, Journal of building engineering 30 (2020), 101228, https://doi.org/10.1016/j.jobe.2020.101228.
[11] A. Farahbakhshtooli, A.K. Bhowmick, Seismic collapse assessment of stiffened steel plate shear walls using FEMA P695 methodology, Eng. Struct. 200 (2019), 109714, https://doi.org/10.1016/j.engstruct.2019.109714.
[12] V. Toufigh, A. Arzeytoon, Quantification of seismic performance factors for ribbed bracing system, Eng. Struct. 176 (2018) 159–174, https://doi.org/10.1016/j.engstruct.2018.08.099.
[13] F. Fattahi, S. Gholizadeh, Seismic fragility assessment of optimally designed steel moment frames, Eng. Struct. 179 (2019) 37–51, https://doi.org/10.1016/j.engstruct.2018.10.075.
[14] S. Mazzoni, F. McKenna, M.H. Scott, G.L. Fenves, B. Jeremic, *OpenSees Command* Language Manual, 2007.
[15] ASCE/SEI 7–16, Minimum Design Loads for Buildings and Other Structures, American Society of Civil Engineers, Virginia, 2016.
[16] AISC 360–16, Specification for Structural Steel Buildings, American Institute of Steel Construction, Chicago, 2016.
[17] AISC 341-16, Seismic Provisions for Structural Steel Buildings, American Institute of Steel Construction, Chicago, 2016.
[18] ASTM A416/A416M-18, Standard Specification for Low-Relaxation, Seven-Wire Steel Strand for Prestressed Concrete, ASTM International, West Conshohocken, PA, 2018.
[19] L.F. Ibarra, R.A. Medina, H. Krawinkler, Hysteretic models that incorporate strength and stiffness deterioration, Earthq. Eng. Struct. Dynam. 34 (2005) 1489–1511, https://doi.org/10.1002/eqe.495.
[20] D.G. Lignos, H. Krawinkler, Deterioration modeling of steel components in support of collapse prediction of steel moment frames under earthquake loading, J. Struct. Eng. 137 (11) (2011) 1291–1302, https://doi.org/10.1061/(ASCE)ST.1943-541X.0000376.
[21] Peer/Atc 72-1, Modeling and Acceptance Criteria for Seismic Design and Analysis of Tall Buildings, Applied Technology Council. Redwood, California, October 2010.
[22] A. Gupta, H. Krawinkler, Seismic Demands for Performance Evaluation of Steel Moment Resisting Frame Structures. Technical Report 132. The John A. Blume Earthquake Engineering Research Center, Department of Civil Engineering, Stanford University, Stanford, CA, 1999.
[23] ASCE/SEI 41-17, Seismic Evaluation and Retrofit of Existing Buildings, Federal Emergency Management Agency, Reston, Virginia, 2017.